POTASSIUM ION ACCUMULATION AT THE EXTERNAL SURFACE OF THE NODAL MEMBRANE IN FROG MYELINATED FIBERS

N. MORAN, Y. PALTI, E. LEVITAN, AND R. STÄMPFLI, *Department of Physiology and Biophysics, Faculty of Medicine-Technion, Haifa, Israel*

ABSTRACT Potassium accumulation associated with outward membrane potassium current was investigated experimentally in myelinated fibers and analyzed in terms of two models—three-compartment and diffusion in an unstirred layer. In the myelinated fibers, as in squid giant axons, the three-compartment model satisfactorily describes potassium accumulation. Within this framework the average space thickness, θ, in frog was 5,900 ± 700 Å, while the permeability coefficient of the external barrier, P_{K_e} was (1.5 ± 0.1) × 10^{-2} cm/s. The model of ionic diffusion in an unstirred aqueous layer adjacent to the axolemma, as an alternative explanation for ion accumulation, was also consistent with the experimental data, provided that D, the diffusion constant, was (1.8 ± 0.2) × 10^{-6}cm/s and l, the unstirred layer thickness, was 1.4 ± 0.1 μm, i.e., similar to the depth of the nodal gap. An empirical equation relating the extent of potassium accumulation to the amplitude and duration of depolarization is given.

The concentration of potassium ion at the outer surface of a number of excitable cells was shown to increase significantly during outward potassium current flow associated with membrane depolarization (13, 8, 9, 10, 25, 12, 19).

The rate of this potassium accumulation, which alters the ionic driving force, is similar to the rate of turn-on or turn-off of the potassium channel. Therefore, it often interferes with the analysis of the conductance kinetics of this channel (23, 11).

This potassium ion accumulation indicates that the fraction of membrane current, flowing through the membrane into the external "space," carried by potassium ions is greater than the corresponding fraction of the current flowing from the space into the bulk medium.

Two models were proposed to account for this phenomenon: (*a*) A three-compartment model consisting of the fiber, the external space and the bulk solution (13). The compartments are separated by two membranes: the excitable membrane and an external barrier or a functional membrane separating the external space from the bulk solution (14, 29, 4). The accumulation is due to the difference between the potassium ion transport numbers through the two membranes. (*b*) Unstirred layer model (13). Within this framework the potassium ions, which carry most of the outward going current, accumulate at the external membrane surface because of the relatively slow mixing of the contents of the aqueous layer adjacent to the membrane, with the bulk solution.

Analysis of the experimental data obtained from squid giant axons led Frankenhaeuser and Hodgkin (13) to the conclusion that the multicompartment model fits the data best. Using a number of simplifying assumptions, they solved analytically the three-compartment model

Dr. Stämpfli's address is the First Physiological Institute, Saarland University, Homburg, West Germany.

equation and estimated the thickness of the external space, θ, in the squid (*Loligo forbesi*) to be ~300 Å and the apparent potassium permeability of the external barrier, P_{K_s}, to be $\sim 6 \times 10^{-5}$ cm/s. Adelman and Palti (2) (see also reference 22), computed numerically in detail the potassium ion accumulation in the space during voltage clamp depolarizations and estimated $\theta = 360 \pm 130$ Å and $P_{K_s} = (3.2 \pm 1.2) \times 10^{-4}$ cm/s (*L. pealei*). The above values of θ are in fair agreement with the anatomical thickness of the Schwann space seen in the squid between the axolemma and the Schwann cell layer. Indeed, the space thickness parameter, θ, was shown to increase by bathing the axon in hypertonic media (3). Such a result is consistent with an increase in the perimeter of Schwann cells layer, i.e., with the widening of the anatomical space at the expense of osmotic shrinkage of the cells. It was, therefore, reasonable to assume that the potassium ion accumulation was indeed due to the anatomical structure of this preparation (4).

Potassium ion accumulation in the space has also been reported in *Myxicola* giant axons (10). However, the values of equivalent space thickness, which were estiamted here, on the basis of a set of restricting assumptions, were significantly larger ($\theta = 2{,}240 \pm 740$ Å). This difference was attributed to an anatomical difference: a wider space and more loosely packed external sheath cells.

In contrast to the above giant axons there is no anatomical evidence for an existence of a similar continuous external barrier around the nodal membrane of myelinated fibers. Nevertheless, in a preliminary report, Palti et al. (25) described significant potassium accumulation in the voltage-clamped frog node. Dubois and Bergman (12) estimated the apparent space thickness at a specific node studied with a depolarization of 140 mV to be ~3,000 Å.

In view of the above, it is the purpose of this work to study and analyze the potassium ion concentration changes at the external membrane surface of the frog node.

METHODS

Experimental

Single myelinated fibers, isolated from the frog *Rana esculenta,* were mounted and voltage-clamped as described by Nonner (20). The node was externally perfused with Ringer's solution containing 60–300 nM tetrodotoxin (TTX). The pH was adjusted to 7.4 by Tris buffer. The temperature was held constant at 15°C.

In between voltage clamp pulses, membrane potential was held at its resting value, V_H. (All potentials are given relative to the resting potential, depolarization is positive, while hyperpolarization is in the negative direction.) At the end of each experiment the node was destroyed by a strong hyperpolarization and the absolute membrane potential, E_M, was determined.

The command voltage pulses were generated by a D/A converter under computer program control. Membrane currents were filtered by a 40-kHz low pass filter and sampled at 20 μs intervals by means of a 10-bit A/D converter operating also under program control (23). The baseline current, sampled for 640 μs before the beginning of the voltage pulses, was averaged and subtracted from all currents analyzed.

Leakage current was assumed to be carried mainly by potassium ions, (15) and was therefore included in the potassium membrane current. Note that Århem et al. (31) showed that at least close to the resting membrane potential, the fraction of membrane current carried by chloride ions is negligible. Since the internal solution in our preparation is close to isotonic KCl (23) and we are concerned only with outward currents, they must be carried mainly by potassium ions.

Analytical

DETERMINATION OF V_K The changes in space potassium concentration were estimated from the changes in V_K, (the potassium reversal potential) determined as a function of the duration of the conditioning depolarization.

V_K was determined by the "tail-current" method (16) i.e., by application of pairs of pulses, each consisting of a depolarizing conditioning prepulse, V_{pp}, immediately followed by a test pulse, V_p. The current elicited by the test pulse is termed the "tail" current.

The "zero-time-tail-current," I_o, was obtained by extrapolating the initial (excluding the capacitive current) exponential portion of the "tail" current to zero time (instant of step from V_{pp} to V_p). Interval between pairs was 2 s. Each prepulse, of a given amplitude and duration, was coupled with a number of test pulses, the amplitudes of which were chosen so as to generate potassium currents close to their reversal potential.

The initial values of the tail currents, I_o, are plotted as a function of test pulse potential, V_p, to give a series of instantaneous *I-V* curves in Fig. 1. The potentials at which these curves cross the abscissa are assumed to correspond to the V_K values at the end of each prepulse.

COMPUTATION OF SPACE PARAMETERS Within the framework of the three-compartment model two parameters define the ion accumulation in the space, namely, θ, the space thickness, and P_{K_s}, the apparent permeability of the external barrier.

Let δK_s denote the excess of potassium in the space over its concentration in the external bulk solution (in Molar). δK_s is given as a function of time, t, by means of the two parameters, θ and P_{K_s}, by the following differential equation (3):

$$d\delta K_s/dt = \frac{I_K}{F}(1 - t_{K_s}) - P_{K_s}\delta K_s/\theta, \tag{1}$$

where I_K is the density of membrane current carried by K^+ ions (mA/cm^2) (the current density for the myelinated fiber has been calculated using the measured fiber length, assuming the node area to be 50 μm^2 (21) and the axoplasmic specific resistance 110 Ωcm), P_{K_s} the apparent permeability of the external barrier (cm/s), θ the space thickness (cm), t_{K_s} the transport number of K^+ in the solution within the space, given by: $t_{K_s} = K_s/\Sigma[\text{anion}]_s + [\text{cations}]_s)$, and F the Faraday constant.

When potassium accumulation in space reaches steady state, $d\delta K_s/dt = 0$, and assuming $\theta \neq 0$, P_{K_s} can be calculated directly, on the basis of Eq. 1, using the following relationship:

$$P_{K_s} = \frac{I_{K_{ss}}(1 - t_{K_{ss}})}{F\,\delta K_{ss}}, \tag{2}$$

the subscript *ss* denoting steady state values in the space. On the other hand, both parameters, θ and P_{K_s}, can be evaluated simultaneously from the time courses of potassium current, I_K, and the corresponding concentration changes in the space, δK_s. This was done by finding the minimum of Φ; the sum of squares of deviations from zero of the integrated form of the material balance equation (Eq. 1) with respect to θ and P_{K_s} (27):

$$\Phi = \sum_{t_u}^{t_2} = (\Delta^2 u_{t_1+2.25})^2, \tag{3}$$

where Δ_u is defined as:

$$\Delta_u = \theta(\delta K_{s_{t_u}} - \delta K_{s_{t_1}}) - \int_{t_1}^{t_u}\left[\frac{I_K}{F}(1 - t_{K_s}) - P_{K_s}\delta K_s\right]dt, \tag{4}$$

where t_1, the shortest prepulse duration used, was between 1 and 3 ms; t_2, prepulse duration, was between 12 and 15 ms (both t_1 and t_2 are within the transient of accumulation); t_u is a variable increasing by Δt from the initial value of t_1 + 2.25 ms, up to t_2; Δt had the following values: 0.15 ms up to t_u = 5 ms, 0.3 ms up to t_u = 10 ms, and thereafter 1.0 ms.

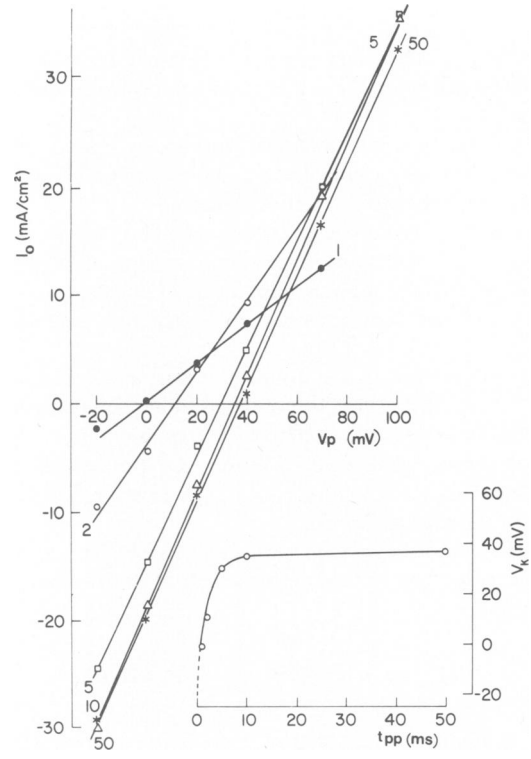

FIGURE 1 Instantaneous *I-V* relationships for different depolarizing prepulse durations, t_{pp}. The points correspond to amplitude of zero-time-tail-currents, I_o, elicited when membrane potential was stepped from a prepulse, V_{pp}, of 100 mV to various test-pulses, V_p. Values of prepulse duration, t_{pp}, (in milliseconds) are given adjacent to each line. (*Inset*) V_K shift as a function of t_{pp}; symbols denote zero-cross-over points of the instantaneous *I-V* relationships. Fiber 4973.

RESULTS

Fig. 1 illustrates the changes in the potassium reversal potential, V_K, indicated by the zero-crossover-points of the instantaneous *I-V* curves, as a function of conditioning depolarization duration, t_{pp} (see inset). As depolarization lengthens, V_K becomes more positive, indicating growing potassium concentration outside the membrane. This is assuming that internal K^+ remains constant because, owing to the high $[K_{in}]/[K_o]$, the larger axoplasmic potassium transport number and larger axoplasmic area available for diffusion, any change in the potassium concentration would produce a much larger V_K shift when it occurs on the outside.

Fig. 1 also shows potassium conductance, G_K, as reflected by the slope of the instantaneous *I-V* curves. The conductance increases at least during the first 5–10 ms, while the outward currents often begin to decay already after 5 ms. Therefore, the decrease in current at the said time, which occurs while G_K increases, must be due to the decrease in driving force rather than to a potassium conductance inactivation.

Fig. 2 compares the shifts of V_K, accompanying an outward current during membrane depolarization in two different types of nerve fibers: a giant axon of the squid and a

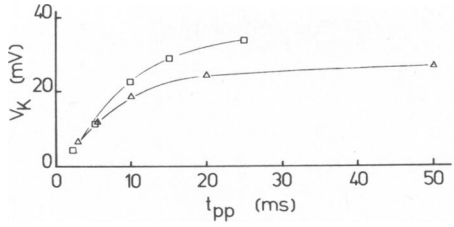

FIGURE 2 V_K shifts in frog node and squid giant axon during comparable depolarizing pulses, V_{pp}, as a function of prepulse duration, t_{pp}. (Δ) myelinated fiber of frog (fiber 5373, V_{pp} = 70 mV); (□) giant axon of squid (from Fig. 2 *a* of Palti et al., 1972; E_H = −59 mV, V_{pp} = 65 mV).

myelinated fiber of the frog. In both, similar depolarizing pulses (65–70 mV) evidently result in a comparable increase in potassium concentration at the external surface of the membrane. This potassium concentration can be computed from V_K by means of the Nernst relationship. As both ends of the frog fiber were cut short and immersed in 117 mM KCl solution for over 20 min, the inner potassium concentration for the node was assumed to be 117 mM (24). In this particular example, after a conditioning depolarization of 65–70 mV the changes of V_K correspond to an ~8- to 10-fold change in external K^+ concentration, i.e., from 2.5 to 21.5 mM in the frog and from 10 to ~96 mM in the squid. (The experimental V_K values used here were taken from reference 22.) This accumulation process is subsequently analyzed in terms of both the three-compartment and diffusion-in-an-unstirred-layer models.

The Apparent Permeability of the External Barrier

The apparent permeability of the external barrier, P_{K_s}, can be determined by means of Eq. 2 from steady state potassium accumulation, or (together with the space thickness, θ) from the transients in potassium current and potassium accumulation using a minimization procedure (see Methods).

The values of P_{K_s}, measured for different depolarizations in myelinated fibers in steady state, are listed in Table I.

The mean P_{K_s} value, obtained for depolarization of 40 mV, is significantly lower than those obtained for depolarizations of 70 and 100 mV in the same fibers. For other potentials, judging by the mean P_{K_s} values of all fibers in each case, the permeability of the external barrier seems unaffected by the magnitude of membrane depolarization. However, since at least two potentials were tested in each fiber, the comparison could be carried out in each fiber separately, using the correlated-pairs test. This test shows that the P_{K_s} values, obtained during depolarization of 50 mV (1.3×10^{-2} cm/s on the average) are smaller by $(0.81 \pm 0.38) \times 10^{-2}$ cm/s and $(1.00 \pm 0.52) \times 10^{-2}$ cm/s, as compared with those obtained for depolarization of 125 and 175 mV, respectively. (These and subsequent deviations are SEM.) The level of significance of these differences being nonzero is 2.5% and 10%, respectively. The same test also shows that the P_{K_s} values, obtained during depolarization of 40 mV (1.2×10^{-2} cm/s on the average) are smaller by $(0.42 \pm 0.11) \times 10^{-2}$ cm/s and by $(0.29 \pm 0.12) \times 10^{-2}$ cm/s, as compared with those obtained for depolarizations of 70 and 100 mV, respectively. The level of significance of the deviations from zero of these differences is 0.5% and 2.5%, respectively. For other pairs of voltages the deviation from zero of these differences is clearly insignificant. Such an increase in P_{K_s} may be due to the relatively large increase in electrokinetic volume

TABLE I

P_{K_s}* AS A FUNCTION OF V_{pp} IN FROG NODE

Fiber	P_{K_s} (cm/s) × 10^2							
	V_{pp}, 40 mV	V_{pp}, 50 mV	V_{pp}, 70 mV	V_{pp}, 100 mV	V_{pp}, 125 mV	V_{pp}, 150 mV	V_{pp}, 175 mV	V_{pp}, 300 mV
4673(*S*)	1.3		2.2	2.1				
4773(*S*)	1.3		1.9	1.5				
4873(*M*)	.81		1.1	.97				
4973(*S*)	1.0		1.3	1.1				
5073(*M*)	1.5		1.9	2.2				
5173(*M*)	0.88		0.81	0.91				
5273(*S*)	1.4		1.4	1.3				
5373(*S*)	.96		1.3	1.0				
5573(*S*)	1.4		1.7	1.5				
5673(*M*)	1.6		2.0	2.5				
5773(*S*)	1.3		2.5	2.4				
6076(*M*)		0.71			0.96		0.89	
6176(*M*)		2.4			4.4		4.9	
6276(*M*)		0.66			0.82		0.83	
6376(*M*)		0.96			1.2		1.1	
6476(*S*)		1.1			3.3		3.1	
6576(*M*)		1.1			1.3			1.2
6776(*S*)		2.2			3.0			1.6
7877(*M*)						0.91		1.3
7977(*M*)						1.4		1.5
8077(*M*)						1.8		2.0
8277(*M*)						2.1		1.0
8377(*M*)						2.2		0.81
8577(*M*)						1.0		1.5
8677(*M*)						1.5		1.7
Mean±SEM	1.2 ± 0.1	1.3 ± 0.3	1.6 ± 0.2	1.6 ± 0.2	2.1 ± 0.5	1.6 ± 0.2	2.2 ± 0.8	1.4 ± 0.1

S and *M* in brackets denote sensory and motor fibers, respectively.

*Determined from the steady state currents and V_Ks.

flow accompanying the outward potassium currents at these high depolarizations. These electrokinetic volume flows may be expected to alter the geometry of the perinodal spacebounding structure, as argued for the intercellular Schwann layer clefts surrounding the giant axon of the squid (1).

When all the data of Table I is pooled together we get (from steady state determination) a mean $P_{K_{s(ss)}}$ value of (1.5 ± 0.1) × 10^{-2} cm/s.

Table II summarizes the values of P_{K_s} obtained by the two independent methods from 13 fibers. Taking all four V_{pp}s, the average P_{K_s} obtained from the transient, $P_{K_{s(t)}}$ = (1.7 ± 0.1) 10^{-2} cm/s, i.e., not very different from the above $P_{K_{s(ss)}}$. However, analyzing the same data using the correlated pairs test, the P_{K_s} values determined from steady-state are found to be significantly smaller than those obtained from fitting the transient at (1.5 % level of significance).

The P_{K_s} value obtained by Dubois and Bergman (12) (1.9 × 10^{-2} cm/s) from the transient of accumulation is compatible with our corresponding average value (1.7 × 10^{-2} cm/s).

TABLE II

APPARENT BARRIER PERMEABILITY, P_{K_s},* AND SPACE THICKNESS, θ, IN MYELINATED FIBERS

Fiber	P_{K_s} (cm/s) × 10^2		θ (Å)	P_{K_s} (cm/s) × 10^2		θ (Å)
	(*ss*)	(*tr*)		(*ss*)	(*tr*)	
	V_{pp}, 70 mV			V_{pp}, 100 mV		
4673	2.2	2.6	4,000	2.1	2.4	7,800
4773	1.9	—	—	1.5	2.1	1,300
4873	1.1	1.0	9,200	0.97	0.87	12,000
4973	1.3	1.5	880	1.1	1.1	4,500
5073	1.9	1.7	4,600	2.2	2.4	5,400
5173	0.81	1.0	3,200	0.91	0.97	5,900
5273	1.4	1.2	10,000	1.3	1.4	6,700
5373	1.3	1.6	9,100	1.0	1.2	5,400
5573	1.7	2.0	3,100	1.5	1.8	3,800
5673	2.0	2.0	12,000	2.5	2.7	2,800
5773	2.5	2.3	2,700	2.4	2.9	3,200
	V_{pp}, 150 mV			V_{pp}, 250 mV		
7877	0.91	0.98	3,400	0.95	0.97	5,600
7977	1.4	1.6	9,400	1.2	1.4	1,000

*The P_{K_s} values were evaluated by two independent methods: *ss*, from the steady state currents and V_Ks, and *tr*, from the transients in their time courses.

The Apparent Space Thickness and V_K Reconstruction

Table II lists the apparent space thickness, θ, in 13 myelinated fibers. The average thickness in these fibers is 5,900 ± 700 Å. The value of θ (2,900 Å) obtained by Dubois and Bergman (12) is about half that of our average value.

To check the predictive power of the three-compartment (two-parameter) model, the model was used to reconstruct the V_K changes from outward potassium currents measured during various depolarizations. The reconstruction was carried out by numerically solving Eq. 1, and converting the concentrations in the space into equilibrium potentials by means of the Nernst relationship.

Fig. 3 *A* is an example of a comparison between the reconstructed V_K shifts (computed from the time course of potassium current generated by a 100 mV depolarizing pulse), with the experimentally determined V_K values (symbols). The continuous line represents the numerical solution of Eq. 1 using the parameters evaluated between 1 and 12 ms. The fit between the experimental data and model predictions was similar to that shown in Fig. 3 *A*, in the 13 fibers investigated. Consequently, it may be concluded that the three-compartment model adequately describes changes in V_K in the frog node.

Simple Diffusion in an Unstirred Layer

In view of the anatomical structure of the node, it seems possible that in the frog the accumulation may be due solely to the discontinuity of ion-transport number in the path of electrical current flow, accompanied by slow mixing at the surface (13, 6).

V_K shifts, computed within the framework of the above model (see Appendix A) are

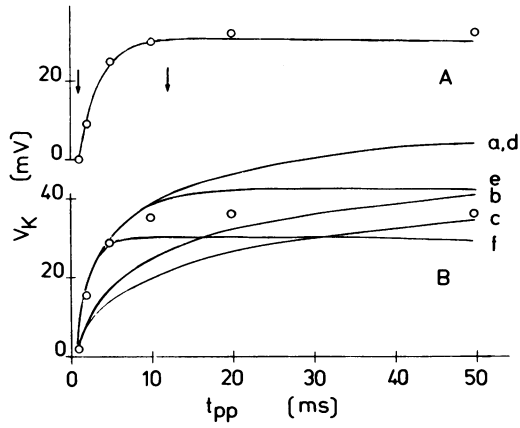

FIGURE 3 The time courses of potassium reversal potential, V_K, in a myelinated fiber depolarized by a 100-mV pulse. Symbols: the experimental values of V_K, (*A*) V_K shifts calculated from outward potassium currents on the basis of the three-compartment model (P_{K_z} = 2.4 × 10^{-2} cm/s, θ = 7,800 Å, as evaluated from the experimental data in the region deliminated by the vertical arrows). Fiber 4673. (*B*) V_K shifts calculated on the basis of the diffusion-in-an-unstirred-layer-model; (*a*) $D = 2 \times 10^{-6}$ cm²/s, (*b*) $D = 1 \times 10^{-5}$ cm²/s, (*c*) $D = 1.8 \times 10^{-5}$ cm²/s (all three with l = 100 μm), (*d*) $D = 2 \times 10^{-6}$ cm²/s and l = 5μm, (*e*) $D = 2 \times 10^{-6}$ cm²/s and l = 2 μm, (*f*) $D = 2 \times 10^{-6}$ cm²/s, l = 1 μm. The reconstruction started at the first experimental V_K point (t_{pp} = 1 ms). Fiber 5273.

compared with those determined experimentally in Fig. 3 *B*. In the figure the computed lines were all made to originate at the first experimental point. It is seen that out of the reconstructed curves, one (curve *e*), based on $D = 2 \times 10^{-6}$ cm²/s and l = 2 μm, fits the time course and to a lesser extent the steady-state value, reasonably. The curves with different values of D and l are not compatible with the experimental points.

The values of D and l were evaluated for 17 fibers by comparing the computed and experimental results (the initial V_K was computed from the K^+ concentration ratio). The average values thus obtained are (1.8 ± 0.2) × 10^{-6} cm²/s and 1.4 ± 0.1 μm, respectively. Note that the above value of D (1.8 × 10^{-6} cm²/s) is 1/10 that of potassium ions in water, and the value of l is roughly equal to the myelin thickness.

V_K Changes with Depolarization: An Empirical Equation

Table III lists the average V_K values (±SEM), experimentally determined in 17 motor fibers, for seven depolarizing pulses of eight durations. On the basis of this data we will derive an empirical equation relating the V_K values to the magnitude and duration of depolarization.

The dependency of V_K on depolarizing pulse duration, t_{pp}, is illustrated in Fig. 3 *A*. This saturation-type function may be described by the following expression:

$$V_{K(t_{pp},V_{pp})} = \frac{V_\infty}{1 + K_1/t_{pp}} + C, \tag{5}$$

where C is the initial value of V_K at t_{pp} = 0. (In our case, since K_{in} = 117 mM and K_o = 2.5 mM, $C \simeq -25$ mV); V_∞ is the steady-state value of V_K shift from C, attained at any depolarization for $t_{pp} \rightarrow \infty$; and K_1 is the time required for the V_K shift to reach half its steady-state value at that depolarization.

TABLE III

POTASSIUM REVERSAL POTENTIAL, V_K, AS A FUNCTION OF MEMBRANE DEPOLARIZATION, V_{PP}, AND ITS DURATION, t_{PP}, IN *R. ESCULENTA*

t_{pp}	V_{pp}						
	50 mV	70 mV	100 mV	125 mV	150 mV	175 mV	250 mV
2	—	14.1 ± 1.3(4)	13.3 ± 1.8(4)	—	17.5 ± 2.5(2)	—	25.0 ± 3.0(2)
3	6.5 ± 1.6(11)	9.0 (1)	14.5 (1)	24.5 ± 3.0(6)	22.4 ± 1.2(7)	35.7 ± 4.2(6)	31.3 ± 3.8(2)
5	—	12.8 ± 1.8(4)	19.6 ± 2.0(4)	—	—	—	—
7	—	—	—	—	38.5 ± 4.5(2)	—	40.5 ± 6.5(2)
10	—	16.3 ± 1.9(4)	24.5 ± 3.1(4)	—	—	—	—
20	—	18.9 ± 2.7(4)	26.6 ± 3.9(4)	—	—	—	—
30	1.0 ± 1.3(8)	—	—	37.8 ± 3.8(6)	36.7 ± 2.3(7)	44.8 ± 4.3(6)	48.5 ± 3.5(2)
50	—	18.9 ± 1.5(4)	28.0 ± 3.9(4)	—	—	—	—

The V_K values are means ± SEM, in millivolts. Numbers in brackets indicate number of fibers used for averaging.

The validity of Eq. 5 for the description of the experimental data can be readily tested by means of its linear form:

$$\frac{1}{V_K - C} = \frac{1}{V_\infty} + \frac{1}{t_{pp}} \cdot \frac{K_1}{V_\infty}. \tag{6}$$

Fig. 4 *A* illustrates that when the experimental data for a depolarization of 100 mV from Table III is inserted into Eq. 6, one gets a linear relationship. The given straight line was fitted to all experimental points, excluding that of the shortest t_{pp}, by the least squares method. Similarly, linear relationships could be demonstrated for the V_K shifts measured at depolarizations of 70 and 150 mV.

Let us now examine the dependency of the parameters of Eq. 5 on the magnitude of depolarization.

The value K_1 may be evaluated at any membrane depolarization from data of Table III by means of yet another form of Eq. 5:

$$K_1 = \left(\frac{V_\infty}{V_K + 25} - 1\right) t_{pp}. \tag{7}$$

The values of K_1 thus obtained, for t_{pp}s $\leq$ 5 ms, are plotted in Fig. 4 *B*, as a function of membrane depolarization. The figures show that, to a good approximation, K_1 is voltages independent.

In contrast, the value of the remaining parameter, V_∞, varies with depolarization, saturating at high membrane potentials. As seen in Fig. 4 *C* it can be described by the following expression:

$$\frac{1}{V_\infty} = \frac{1}{V_{Max}} + \frac{1}{V_{pp}} \cdot \frac{K_2}{V_{Max}}, \tag{8}$$

which is the linear form of the simple equation

$$V_\infty = \frac{V_{Max}}{1 + K_2/V_{pp}}, \tag{9}$$

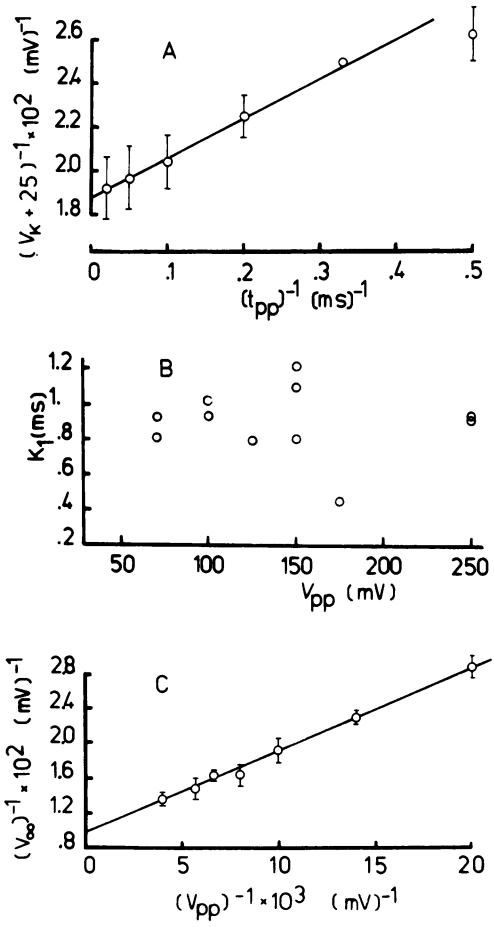

FIGURE 4 The empirical equation; validity of the relationship (Eq. 10) and voltage dependency of the parameters. (*A*) The reciprocal values of V_K shift, $(V_K + 25)^{-1}$ as a function of the reciprocal of depolarizing pulse duration, $(t_{pp})^{-1}$. The straight line was fitted to the experimental points (the shortest t_{pp} excluded) by the least squares method. V_{pp} = 100 mV. Data from Table III. (*B*) Half shift time of V_K, K_1, as a function of membrane potential, V_{pp}. K_1 was calculated by means of Eq. 7 for depolarizing pulse durations between 2 and 5 ms. Data from Table III. (*C*) The reciprocal of V_∞, $(V_\infty)^{-1}$ as a function of the reciprocal of V_{pp}, $(V_{pp})^{-1}$. The lines were fitted to the experimental points by the least squares method. Data from Table III.

where V_{Max} is the saturation value of V_∞ and K_2 is the value of membrane depolarization at which V_∞ attains the value of $V_{Max}/2$.

Consequently, the relationship between the V_Ks and the amplitude and duration of a depolarizing pulse may be expressed by the following empirical equation:

$$V_{K(t_{pp},V_{pp})} = \frac{V_{Max}}{1 + K_2/V_{pp}} \cdot \frac{1}{1 + K_1/t_{pp}} - 25. \qquad (10)$$

The three parameters of Eq. 10, K_1, K_2, and V_{Max}, were evaluated simultaneously by fitting this equation to the experimental data of Table III. This was done by minimizing the sum of

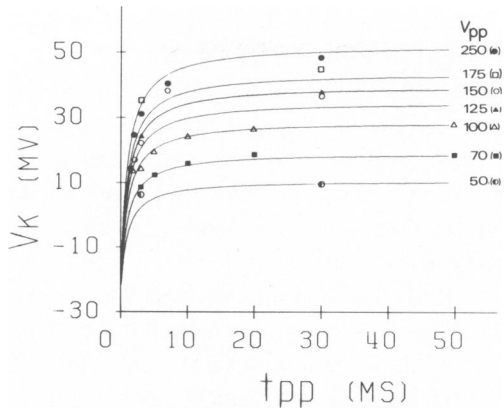

FIGURE 5 Values of V_K as a function of the duration of depolarization, t_{pp} and its amplitude, V_{pp}. Symbols: experimental values of V_K (from Table III), determined at the following membrane potentials (in millivolts): ◐:50, ■:70, △:100, ▲:125, ○:150, □:175, and ●:250. Lines: V_K values computed using Eq. 6, for depolarizations as denoted near each line (in millivolts). The equation parameters found to fit best the above data were: $K_1 = 0.95$ ms, $K_2 = 102$ mV, $V_{Max} = 109$ mV.

squares of deviations of the calculated V_Ks from the experimental points. The least reliable V_K values were excluded, namely, $V_{pp} = 50$ mV and $t_{pp} \leq 3$ ms and $V_{pp} = 70$ mV and $t_{pp} \leq 2$ ms.

Fig. 5 presents the experimental (symbols) and calculated (using Eq. 10) values of V_K, as a function of duration and amplitude of the depolarization.

It is seen that the experimental points (excluding those of the lowest V_{pp}s and shortest t_{pp}s) are reasonably well described by Eq. 10 with the following parameters: $K_1 = 0.95$ ms, $K_2 = 102$ mV, and $V_{Max} = 109$ mV.

DISCUSSION

The process of ion accumulation in frog myelinated fibers as studied in this work seems to be well described by the three-compartment (two-parameter) model. While in the squid giant axon this model is apparently consistent with the anatomical structure, i.e., the existence of an aqueous periaxonal space externally bounded by a cellular layer (13, 30, 4), in myelinated fibers the structural basis for this model is not obvious. The nodal gap is surrounded by a thick collar formed by numerous processes of the neighboring satellite Schwann cells (18). However, a continuous cellular bounding structure has not been described. This morphological difference may account for the difference in the values of the space parameters, which for the myelinated fiber are at least an order of magnitude larger than those of the giant axons. In view of the above, the similarity in accumulation rates between the giant axons and the frog nerve (Fig. 2) seems unexpected. However, the relatively rapid accumulation rate at the node results from the fact that the slowing effect of the larger space here is being compensated by the current density which is 10–20 times greater than in giant axons.

While the three-compartment model is in very good agreement with the experimental data, the large thickness of the apparent space surrounding the node seems to partially invalidate one of the basic assumptions of this model, namely, instantaneous mixing in the space (the time constant of mixing here is ~1 ms). Therefore it may be useful to test the data against

some other possible models, and specifically the model of unidimensional diffusion in an unstirred layer.

It is generally accepted that the thickness, l, of an unstirred layer adjoining a membrane is of the order of 100 μm (28). However, Fig. 3 *B* shows that when this value is used together with the value of the diffusion constant of potassium in an aqueous solution (1.8×10^{-5} cm/s in a 0.1 M KCl solution at 25°C), the model fails to describe the experimental data (line *c*). Considering the possibility of a slowing down of K^+ diffusion in the vicinity of the node, the computation was repeated with D values going down to 2×10^{-6} cm^2/s. It is seen that the fit does not improve (lines *a* and *b*). With these values of D the unstirred layer model predicts, in the best case, either a somewhat slower rate of accumulation at depolarizations of the shortest durations or excessive accumulation at the longest durations. Changing l in the range of 10–500 μm does not affect the outcome of the calculations.

In contrast, the calculated V_K shifts follow the time course of the experimental points rather closely, provided the normal value of D is lowered by a factor of ~10 and l is reduced to 2 μm, equaling roughly the depth of the perinodal gap (line *e*). A further reduction of l leads to underestimation of the accumulation (line *f*). Similar results were obtained in other fibers.

The lower projected diffusion constants may be due to a slower diffusion in a cation-binding medium. Such a medium in the perinodal gap termed "gap substance" or "cementing disc," has been suggested by Landon and Langley (17) to contain protein-linked, carboxylated mucopolisaccharides.

This region of restricted diffusion may be represented by a thin barrier to diffusion with an apparent permeability, $P_{K,}$, given by (13):

$$P_{K,} = \frac{D}{l} = \frac{10^{-6}\ \text{cm}^2/\text{s}}{10^{-4}\ \text{cm}} = 10^{-2}\ \text{cm/s}.$$

This value is very similar to the average $P_{K,}$ value (1.5×10^{-2} cm/s) obtained within the framework of the three-compartment model.

Since both types of accumulation models seem to adequately describe the experimental data, and in view of the presently available anatomical evidence, it may be concluded that the restricted diffusion compartment model represents the discussed nodal behavior and structure. However, further histological studies are required before a final conclusion is reached.

It should be noted that motor myelinated fibers usually display smaller accumulation as compared with sensory fibers. Moreover, four of the 20 motor fibers tested in this series had to be excluded from the analysis because they showed no V_K shifts with time upon depolarization (see also reference 25). It is interesting to note that the possibility of variability in K^+ accumulation has been mentioned by Armstrong and Hille (5), their observation being based on the appearance or absence of tail currents.

The description of accumulation in myelinated fibers in terms of any of the two above models does not permit a simple reconstruction of V_K. One can do so only using numerical analysis methods. Therefore, an empirical equation which provides an analytical immediate solution may prove useful. Note, however, that as less information is used in calculation of V_K by the given empirical equation, Eq. 10 (for example, this calculation does not include the use of the potassium current time course), it may in some cases result only in a fair approximation rather than an exact description of V_K.

However, not all deviations of experimental points from the calculated lines may be ascribed to this general cause. For example, the values of V_K determined for the shortest and lowest depolarizations and which are not fitted by the calculated lines (Fig. 5) deviate systematically in the depolarizing direction. This deviation is due at least in part to the fact that the reversal potential of potassium, determined at the end of such depolarizations, is not an absolutely pure or "true" potassium reversal potential since it reflects a small contribution of the sodium equilibrium potential (see Appendix B).

It may be thus concluded that V_K can be reasonably well described, as a function of depolarizing pulse amplitude and duration, by means of Eq. 10. It should be noted that the parameter values given here are suitable for a preparation under normal conditions. However, it may be assumed that as long as the general shape of both the ionic current time course and the steady-state I-V relationship is preserved, i.e., as long as the experimental conditions affect these currents by a constant factor, the values of the parameters K_1 and K_2 will remain unchanged and only V_{Max} will have to be adjusted.

The parameters K_1 and K_2 may be meaningful to the normal physiological nervous activity. K_1, the time from beginning of depolarization until the V_K shift attains half its steady-state value, is in the range of action potential duration and has a value of ~1 ms. K_2, the membrane potential at which the V_K shift attains half its maximal value, is in the range of membrane potentials during action potential with a value of ~100 mV. V_{Max}, the maximal possible V_K shift, reaches the high value of 109 mV (relative to its value in rest). Consequently, within the duration of the action potential overshoot (lasting ⅓–½ ms) a significant V_K shift may occur, representing a significant potassium accumulation in the immediate vicinity of the nodal membrane.

APPENDIX A

Calculation of potassium concentration at the outer surface of the membrane assuming unrestricted diffusion of ions through an adjoining unstirred layer.

Such diffusion is described by

$$\frac{\delta y}{\delta t} = D\frac{\delta^2 y}{\delta x^2} \tag{A1}$$

where y is the excess of potassium concentration at a distance x from the inner edge of the layer, and D is the diffusion coefficient. Assuming that a unit quantity (per unit area) of potassium ions is liberated instantaneously at $t = 0$ and $x = 0$, and taking the boundary conditions as $\delta y/\delta x = 0$ at $x = 0$ and $y = 0$ at $x = l$, the solution of Eq. A1 for $x = 0$ can be represented by the following series:

$$y_{o,t} = \frac{1}{\sqrt{\pi Dt}}\left(1 - 2e^{-l^2/Dt} + 2e^{-4l^2/Dt} - 2e^{-9l^2/Dt} \ldots\right), \tag{A2}$$

or

$$y_{o,t} = \frac{2}{l}\left(e^{-\pi^2 Dt/4l^2} + e^{-9\pi^2 Dt/4l^2} + e^{-25\pi^2 Dt/4l^2} \ldots\right). \tag{A3}$$

The two series have the same sum. Eq. A2 converges rapidly when t is small, whereas Eq. A3 converges rapidly when t is large. With an error not exceeding 1% it is sufficient to use the first two terms of A2 for

small values ot t:

$$y_{o,t} = \frac{1}{\sqrt{\pi Dt}}(1 - 2e^{-l^2/Dt}), \tag{A4}$$

or two terms of Eq. A3 for large values of t:

$$y_{o,t} = \frac{2}{l}(e^{-\pi^2 Dt/4l^2} + e^{-9\pi^2 Dt/4l^2}). \tag{A5}$$

The external K^+ concentration changes during membrane depolarizations lasting up to 50 ms were calculated by convolving numerically Eqs. A4 and A5 with the potassium outward current (after appropriate conversion of units).

APPENDIX B

Determination of Leakage Conductance Components

The determination of the leakage conductance components G_{Na_L} and G_{K_L} was performed on the basis of the following assumptions: (*a*) The experimentally determined relationship between leakage current I_L and membrane potential V_M is ohmic and crosses the abscissa at V_L, which equals the resting potential. The leakage conductance, G_L, is given by the slope of this line. (*b*) Sodium and potassium currents, I_{Na_L} and I_{K_L}, are the only components of I_L (15). (*c*) The current-voltage relationships of I_{Na_L} and I_{K_L} are linear. The lines describing I_{Na_L} and I_{K_L} vs. V_M cross the abscissa at the respective reversal potentials, V_{Na} and V_K, and their slopes represent the appropriate conductances: G_{Na_L} and G_{K_L}.

From the above it follows that at membrane potential equaling V_K, I_L is carried solely by sodium and at membrane potential equaling V_{Na} I_L consists only of I_{K_L}. Thus, at these two potentials we get

$$G_L(V_K - V_L) = G_{Na_L}(V_K - V_{Na}) \tag{B1}$$

and

$$G_L(V_{Na} - V_L) = G_{K_L}(V_{Na} - V_K). \tag{B2}$$

From these the components of the leakage conductance, G_{Na_L} and G_{K_L}, may be easily extracted. For example, using the values $V_L = 0$, $V_{Na} = 120$ mV, $V_K = -25$ mV, and $G_L = 44$ mS/cm^2, we calculate G_{Na_L} to be 8 mS/cm^2 and $G_{K_L} = 36$ mS/cm^2 (fiber 4973).

Determination of V_K

The apparent potassium reversal potential, experimentally determined in a TTX-treated membrane at various times during a depolarizing pulse, reflects in addition to I_K the varying contribution of sodium component in leakage current. Therefore, the true V_K should be calculated from the apparent V_K.

The experimentally measured total apparent potassium current, $I_{K_{app}}$ can be resolved into a potassium current, I_K and a sodium current, I_{Na_L}. Note that the potassium current consists of the delayed channel current in addition to the potassium component of leakage.

The slopes of these current curves, $G_{K_{app}}$, G_K, and G_{Na_L}, represent the respective conductances. Let $V_{K_{true}}$ be the potassium reversal potential in the depolarized membrane and V_{Na} the sodium reversal potential. Since $V_{K_{app}}$ is the zero-current potential at which the outward potassium current just balances the inward sodium current then

$$G_{Na_L}(V_{K_{app}} - V_{Na}) = -G_K(V_{K_{app}} - V_{K_{true}}). \tag{B3}$$

At a membrane potential equaling V_{Na}, the experimentally measured instantaneous current consists of potassium current only, i.e.

$$G_K(V_{Na} - V_{K_{true}}) = G_{K_{app}}(V_{Na} - V_{K_{app}}), \quad \text{(B4)}$$

$V_{K_{true}}$ may be obtained after substituting G_K from Eq. B4 into Eq. B3 and rearranging:

$$V_{K_{true}} = (V_{K_{app}} - V_{Na}G_{Na_L}/G_{K_{app}})/(1 - G_{Na_L}/G_{K_{app}}).$$

For example, using the above values of V_{Na} and G_{Na_L} with the following values determined experimentally for a 1-ms and 100-mV pulse: $V_{K_{app}} = -1\ mV$ and $G_{K_{app}} = 175\ mS/cm^2$, we obtain $V_{K_{true}} = -7.5$ mV instead of the apparent V_K (−1 mV).

We are greatly indebted to Ofer Binah for his encouragement, support and stimulating discussions during the course of this work. We are also grateful to Dr. M. H. Sherebrin for his help in analyzing the material and to Ms. H. Matalon for typing the manuscript.

This work was supported in part by the Israeli National Academy of Sciences and by Deutsche Forschungsgemeinschaft Sonderforschungsbereich 38 "Membranforschung," and was done in partial fulfillment of the Doctor of Science degree for N. Moran.

Received for publication 10 December 1979 and in revised form 9 May 1980.

REFERENCES

1. ADAM, G. 1973. The effect of potassium diffusion through the Schwann cell layer on potassium conductance of the squid axon. *J. Membr. Biol.* **13**:353–386.
2. ADELMAN, W. J., JR. and Y. PALTI. 1972. The role of periaxonal and perineuronal spaces in modifying ionic flow across neural membranes. *Curr. Top. Membranes Transp.* **3**:199–235.
3. ADELMAN, W. J., JR., Y. PALTI, and J. P. SENFT. 1973. Potassium ion accumulation in a periaxonal space and its effects on the measurement of membrane potassium ion conductance. *J. Membr. Biol.* **13**:387–410.
4. ADELMAN W. J. JR., J. MOSES, and R. N. RICE. 1977. An anatomical basis for the resistance and capacity in series with the excitable membrane of the squid giant axon. *J. Neurocytol.* **6**:621–646.
5. ARMSTRONG, C. M., and B. HILLE. 1972. The inner quaternary ammonium ion receptor in potassium channels of the node of Ranvier. *J. Gen. Physiol.* **59**:388–400.
6. BARRY, P. H., and A. B. HOPE. 1969 *a*. Electroosmosis in membranes: effects of unstirred layer and transport numbers. I. Theory. *Biophys. J.* **9**:700–728.
7. BARRY P. H., and A. B. HOPE. 1969 *b*. Electroosmosis in membranes: effects of unstirred layer and transport numbers. II. Experimental *Biophys. J.* **9**:729–757.
8. BAYLOR, D. A., and J. G. NICHOLLS. 1969 *a*. Changes in extracellular potassium concentration produced by neuronal activity in the central nervous system of the leech. *J. Physiol.* **203**:555–569.
9. BAYLOR, D. A., and J. G. NICHOLLS. 1969 *b*. After-effects of nerve impulses on signalling in the central nervous system of the leech. *J. Physiol.* **203**:571–589.
10. BINSTOCK, L., and L. GOLDMAN. 1971. Rectification in instantaneous potassium current-voltage relations in *Myxicola* giant axons. *J. Physiol.* **217**:517–531.
11. CLEEMAN, L., and M. MORAD. 1979. Potassium currents in frog ventricular muscle: evidence from voltage clamp currents and extracellular K accumulation. *J. Physiol.* **286**:113–143.
12. DUBOIS, J. M., and C. BERGMAN. 1975. Potassium accumulation in the perinodal space of frog myelinated axons. *Pflügers Arch.* **358**:111–124.
13. FRANKENHAEUSER, B., and A. L. HODGKIN. 1956. The after-effects of impulses in the giant nerve fibers of *Loligo*. *J. Physiol.* **131**:341–376.
14. GEREN, B. B., and F. O. SCHMITT. 1954. The structure of the Schwann cell and its relation to the axon in certain invertebrate nerves fibers. *Proc. Natl. Acad. Sci. U.S.A.* **40**:863–871.
15. HILLE, B. 1973. Potassium channels in myelinated nerve. Selective permeability to small cations. *J. Gen. Physiol.* **61**:669–686.
16. HODGKIN, A. L., and A. F. HUXLEY. 1952. The components of membrane conductance in the giant axon of *Loligo*. *J. Physiol.* **116**:473–496.
17. LANDON, D. N., and O. K. LANGLEY. 1971. The local chemical environment of the node of Ranvier. A study of cation binding. *J. Anat.* **108**:419–432.
18. LANDON, D. N., and P. L. WILLIAMS. 1963. Ultrastructure of the node of Ranvier. *Nature (Lond.)*. **199**:575–577.

19. MORAN, N., Y. PALTI, E. LEVITAN, and O. BINAH. 1979. Potassium accumulation in periaxonal space of myelinated fibers and giant axons. *Isr. J. Med. Sci.* **15**:619.
20. NONNER, W. 1969. A new voltage clamp method for Ranvier node. *Pflügers Arch.* **309**:116–192.
21. NONNER, W., E. ROJAS, and R. STÄMPFLI. 1975. Displacement currents in the node of Ranvier, voltage and time dependence. *Pflügers Arch.* **354**:1–18.
22. PALTI, Y., W. J. ADELMAN, JR., and J. P. SENFT. 1972. Modification of membrane currents and potentials by dynamic alterations of ionic concentration in periaxonal space. *Actual. Neurophysiol.* **10**:210–235.
23. PALTI, Y., G. GANOT, and R. STÄMPFLI. 1976. Effect of conditioning potential on potassium current kinetics in the frog node. *Biophys. J.* **16**:261–273.
24. PALTI, Y., R. GOLD, and R. STÄLMPFLI. 1979. Diffusion of ions in myelinated nerve fibers. *Biophys. J.* **25**:17–32.
25. PALTI, Y., R. STÄMPFLI, A. BRETAG, and W. NONNER. 1973. Potassium ion accumulation at the external surface of myelinated nerve fibers. *Isr. J. Med. Sci.* **9**:680.
26. PALTI, Y., N. MORAN, and R. STÄMPFLI. 1980. Potassium currents and conductance: comparison between motor and sensory myelinated fibers. *Biophys. J.* **32**:955–966.
27. POWELL, M. T. D. 1964. An efficient method for finding the minimum of a function of several variables without calculating derivatives. *Computer J.* **7**:155–162.
28. POZNANSKY, M., S. TONG, C. C. WHITE, J. M. MILLGRAM, and A. K. SOLOMON. 1976. Nonelectrolyte diffusion across lipid bilayer systems. *J. Gen. Physiol.* **67**:45–66.
29. VILLEGAS, G. M. 1969. Electron microscopic study of the giant nerve fiber of the giant squid *Dosidicus gigas*. *J. Ultrastruct. Res.* **26**:501–514.
30. VILLEGAS R., C. CAPUTO, and L. VILLEGAS. 1962. Diffusion barriers in the squid nerve fiber. The axolemma and the Schwann layer. *J. Gen. Physiol.* **46**:245–255.
31. ÅRHEM, P. B., B. FRANKENHAUER, and L. E. MOORE. 1973. Ionic currents at resting potential in nerve fibers from *Xenopus laevis*. Potential clamp experiments. *Acta Physiol. Scand.* **88**:446–454.